Investigation of Two-photon LIF of Ground State Neutral Xe for Electric Propulsion Application

IEPC-2017-325

Presented at the 35th International Electric Propulsion Conference
Georgia Institute of Technology • Atlanta, Georgia • USA
October 8 – 12, 2017

Kiyoshi Kinefuchi[1], Yoshio Nunome[2], Shinatora Cho[3], Ryudo Tsukizaki[4]
Japan Aerospace Exploration Agency, Tsukuba, Ibaraki, 305-8505, Japan

Tat Loon Chng[5]
Princeton University, Princeton, NJ, 08544, USA

Abstract: Ion engines and Hall thrusters commonly use xenon as a propellant and several measurement techniques for xenon ions and metastable neutrals have been applied to evaluate the characteristics of the thrusters and to understand the underlying physics. Density measurements of xenon atoms can provide crucial information on the ionization characteristics and help explain charge exchange phenomenon. Two-photon absorption laser induced fluorescence, TALIF, is promising because it allows access to ground state xenon atoms by using around 220 to 260 nm wavelength lasers which have become more readily available lately. In this study, observation of TALIF signals from a room temperature (cold) xenon gas cell is conducted with 249 and 252 nm wavelength excitation at xenon pressures of 0.1 and 10 Torr. TALIF signals are obtained against a wide range of laser intensities, and the resulting fluorescence response comprises of a few regimes – weak-excitation, saturation, and an intermediate regime. The natural lifetime and quenching rate are evaluated by analyzing the fluorescence decay, and the result is consistent with published literature. Finally, actual application to ground tests of Hall thrusters is discussed based on the experimental results, especially with respect to their fluorescence responses.

Nomenclature

A_{ij}	=	Spontaneous emission probability
B_{ij}	=	Stimulated emission and absorption probabilities through two-photon process
I	=	Laser intensity
k	=	Quenching rate constant
N	=	Total number density
N_i	=	Number density of state i
Q	=	Quenching rate
S_F	=	Fluorescence intensity
V	=	Volume of observation region
Ω	=	Solid angle to observation region
τ	=	Time constant

[1] Associate Senior Research Engineer, Space Technology Directorate I.
[2] Associate Senior Research Engineer, Research and Development Directorate.
[3] Research Engineer, Research and Development Directorate.
[4] Assistant Professor, Institute of Space and Astronautical Science.
[5] Researcher, Department of Mechanical and Aerospace Engineering.

I. Introduction

HALL Effect thrusters and ion engines use xenon as a propellant and a number of diagnostics for xenon have been conducted to evaluate the thruster performance and to clarify the physical processes involved. Xenon ions can be detected by physical probe-based techniques like Langmuir probe, RPA (retarding potential analyzer), etc. Emission spectroscopy, laser absorption spectroscopy and LIF (laser induced fluorescence) are applicable not only for xenon ions but also for metastable neutrals[1,2]. If the target wavelength lies within the near infrared, low cost diode lasers can be used, which is an advantage for laser diagnostics.

Measurement of number density of xenon neutrals is of great interest for research and development of xenon electric propulsion because it provides crucial information such as the ionization characteristics around the thruster head and cathode, CEX (charge exchange) ion generation, effect of ground test environment, etc. A comparison of the neutral xenon distribution between a cold flow (without discharge) and hot flow (with discharge) can give detailed information on the ion generation. In general, in Hall thrusters and ion engines, xenon neutrals are not in thermal equilibrium so it is inaccurate to estimate the total number density of xenon neutrals from metastable neutrals assuming Boltzmann equilibrium. An ionization gauge is a possible candidate for measuring neutral total density, but suffers from difficulties in implementation around the thrusters, disturbance to the flow and low spatial resolution. Therefore, to access ground state xenon neutrals using lasers would be a candidate for neutral density measurements. To do this, lasers with around 110 to 130 nm wavelength are needed, but they are expensive and difficult to setup especially since air becomes increasingly opaque below 180 nm. On the other hand, TALIF (two-photon absorption LIF) has been tried for the measurement of ground state neutral xenon[3]. In TALIF, as shown in Fig. 1, lasers with twice the wavelength of the energy level difference can be applicable. That means lasers with around 220 to 260 nm wavelength like Nd:YAG pumped dye laser systems, which are widely used and capable of delivering high energy, can be readily applied for ground state xenon excitation.

Although number density measurement of ground state neutral xenon using TALIF has been already applied to a Hall thruster[4] using saturated LIF, the high laser energies required (6 mJ/pulse), typically involves high cost and a larger scale experimental setup. Instead of saturation fluorescence, operating in the weak-excitation regime is a favorable candidate given that it is less demanding in terms of the laser intensity requirements and consequently implies a lower cost and handier laser system. However, detection of the weak fluorescence is the primary tradeoff. In addition to this, the measurements in Ref. 4 were conducted around the thruster exit, thus, in extending these applications available to TALIF to include measurements inside thrusters[5] and hollow cathodes, optimization of incident laser power would be needed. However, a more detailed examination of the fluorescence response (saturation/weak excitation) over a range of incident laser powers and optimization of these conditions for application towards ground tests of electric propulsion so far have never been done. Therefore, the TALIF experimental specifics for ground state xenon measurements for electric propulsion application has not been established yet and guidelines on the incident laser energy for each xenon number density range and experimental setup are also necessary.

In this study, TALIF experiments in a xenon cold gas cell are conducted with a view to understanding the laser energy requirements and possible issues that may be encountered in the experimental setup for electric propulsion application. The incident laser intensity is swept over a wide range to survey the fluorescence response from the weak-excitation to saturation regime. Two different transitions (i.e. laser wavelengths) and two pressure conditions are tested. In terms of the application to Hall thrusters, characteristics of saturation and weak excitation and their remarks are discussed based on the experimental result.

II. Two-photon Absorption LIF

In TALIF, as shown in Fig. 1, the target particle, here ground state xenon atom, is excited from state 0 to state 2 by a two-photon absorption process. The excited particle is de-excited from state 2 through natural emission, induced emission and quenching, thus,

$$\dot{N}_2 = (N - N_2)B_{02}I^2 - N_2(Q + A + B_{20}I^2) \quad (1)$$

The fluorescence intensity S_F from state 2 to state 1 through natural emission is

$$S_F = V\frac{\Omega}{4\pi}A_{21}N_2 \quad (2)$$

The rise-up time constant τ of fluorescence is

$$\tau = \frac{1}{Q + A + (B_{02} + B_{20})I^2} \quad (3)$$

Here I is the peak value. On the other hand, as for the fall-down time, set $I \sim 0$,

$$S_F \propto exp\{-(A + Q)t\} \quad (4)$$

$$\tau = \frac{1}{Q + A} \tag{5}$$

Assuming equilibrium conditions in Eq. (1), or $\dot{N}_2 = 0$, Eq. (2) turns into the following expression.

$$S_F = V \frac{\Omega}{4\pi} A_{21} N \frac{B_{02} I^2}{Q + A + (B_{02} + B_{20}) I^2} \tag{6}$$

Here $Q = kN$. When $(B_{02} + B_{20}) I^2 \ll Q + A$, Eq. (6) becomes

$$S_F = V \frac{\Omega}{4\pi} A_{21} N \frac{B_{02} I^2}{Q + A} \tag{7}$$

This is commonly known as the weak-excitation regime or weak-excitation fluorescence. In this case, the fluorescence intensity is proportional to the square of the laser intensity. Note that S_F is not simply proportional to the N except in the case $Q \ll A$ because $Q = kN$. When $(B_{02} + B_{20}) I^2 \gg Q + A$, Eq. (6) is expressed as

$$S_F = V \frac{\Omega}{4\pi} A_{21} N \frac{B_{02}}{B_{02} + B_{20}} \tag{8}$$

The fluorescence is just proportional to N, that is, has no dependence on laser intensity. This is saturation fluorescence. When $(B_{02} + B_{20}) I^2 \approx Q + A$, the fluorescence follows Eq. (6), and here it is termed intermediate fluorescence.

III. Experimental Apparatus

Figure 2 shows the experimental setup. A Nd:YAG laser (Spectra Physics Pro250-10) pumps a Coumarin dye laser (Sirah PRSC-LG-24-US) to obtain the desired wavelength. The laser pulse has 10 ns FWHM and 10 Hz repetition frequency. The laser energy is measured by a power meter and the maximum laser energy obtained at the dye laser exit is 10 mJ/pulse. Table 1 summarizes the commonly accessed two-photon transition wavelengths for probing ground state xenon atom using TALIF. In this study, considering the wavelength range of the laser system, 249.63 nm excitation with 828.01 nm fluorescence and 252.49 nm excitation with 823.16 nm fluorescence are the chosen schemes because higher fluorescence intensity is expected. However, for actual application to ground test of electric propulsion, the wavelength should be selected to maximize the measurement accuracy considering not only fluorescence intensity but also background emission of plasma from thrusters.

The laser beam from the dye laser is led into a cold xenon gas cell made of quartz glass through a lens with 50 mm focal length. A lens with a longer focal length cannot be used because the quartz glass would be melted by the focused laser beam. Two gas cells with 0.1 torr and 10 torr xenon pressure are prepared for the experiment.

The fluorescence is detected by means of a photo detector (Thorlabs PDA10A) through an interference filter and two collimating lenses with 50 mm focal length as show Fig. 2. Two interference filters, 820 and 830 nm of center wavelength, are used for each fluorescence, 828.01 and 823.16 nm, respectively. The FWHM of each interference filter is 10 nm. The fluorescence spectra and spectral response of each interference filter are shown in Figs. 3 and 4. Both fluorescence wavelengths and the attendant spectra fall within the transmission range of the interference filters, as seen from Fig. 4.

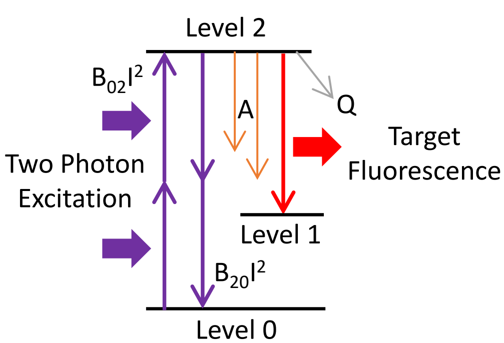

Figure 1. Theoretical schematic of TALIF.

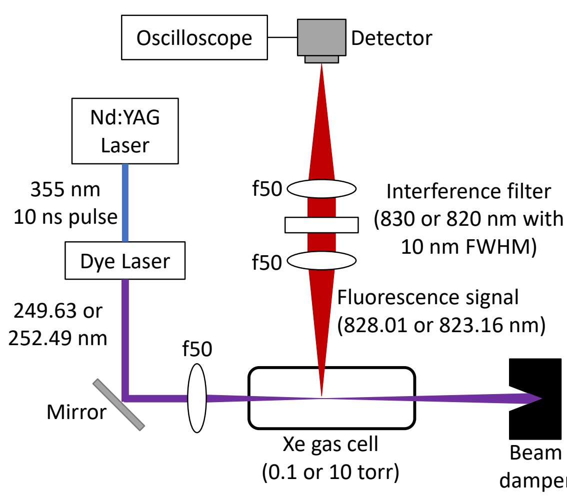

Figure 2. Experimental setup.

Table 1. Candidate transitions of TALIF

Ground State	Excited State	Single Photon Wavelength	Intermediate State	Fluorescence Wavelength	Fluorescence Intensity	Reference
$5p^6$ $^1S_0$	6p’ $[3/2]_2$	224.29 nm	6s’ $[1/2]^o_1$	834.68 nm	2000	3, 6
	7p $[3/2]_2$	225.51 nm	6s $[3/2]^o_2$	462.43 nm	1000	6-8
			6s $[3/2]^o_1$	484.33 nm	300	
			6s’ $[1/2]^o_1$	869.22 nm	100	
	7p $[5/2]_2$	226.37 nm	6s $[3/2]^o_2$	469.70 nm	300	6
	6p $[1/2]_0$	**249.63 nm**	**6s $[3/2]^o_1$**	**828.01 nm**	**7000**	9, 10
	6p $[3/2]_2$	**252.49 nm**	6s $[3/2]^o_1$	895.23 nm	1000	9, 10
			6s $[3/2]^o_2$	**823.16 nm**	**10000**	
	6p $[5/2]_2$	256.02 nm	6s $[3/2]^o_1$	992.32 nm	3000	9-11
			6s $[3/2]^o_2$	904.54 nm	400	

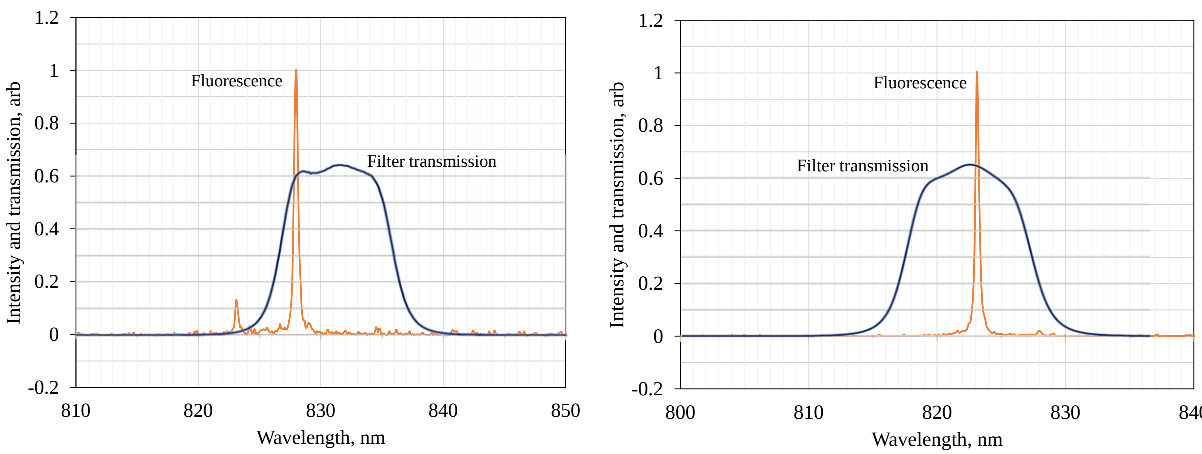

Figure 3. Fluorescence spectra and characteristic of interference filter for 249 nm laser (left) and 252 nm laser (right).

IV. Experimental Results and Discussion

A. 249 nm Laser Excitation

Figure 4 (a) shows fluorescence pulse waveforms against various incident laser energy with 249 nm laser wavelength and 10 Torr xenon cold gas cell. The laser pulse waveform is also shown in the figure. All pulse waveforms are non-dimensionalized by their respective peak values. The data were obtained up to around 10 mJ laser energy, but the fluorescence waveforms are similar in the case of 0.05 mJ and 0.1 mJ, and over 0.1 mJ as well. Therefore, waveforms over 0.1 mJ are not indicated in the figure.

All fluorescence waveforms in Fig. 4 (a) follow laser waveform before reaching the peak because the time constant in Eq. (3) is shorter enough than laser pulse (10 ns). On the other hand, after the peak, the behavior differs with laser energy. In the higher laser energy cases, 0.1 mJ and 0.05 mJ, the fluorescence waveforms follows the laser pulse. However, in the lower laser energy cases, 0.042 mJ and 0.016 mJ, the fluorescence waveforms start to decay with certain delay – in 20 ns at 0.042 mJ and 18 ns at 0.016 mJ. Besides, the fluorescence is maintained even when the laser intensity nearly equals to zero. This behavior seems to follow the time constant in Eq. (5), hence, curve fitting to 0.042 mJ and 0.016 mJ waveforms in the decay period has been conducted based on the exponential decay function of Eq. (4). The result is shown in Fig. 4 (b). In the graph, the time origin is based on t = 0 of the fitted decay function, and the waveforms shown in Fig. 4 (a) are translated in time direction. As shown in Fig. 4 (b), the fluorescence waveforms are successfully fitted to the decay function. Here the time constant of the decay, $1/(A+Q)$, is obtained as 13 ns.

At 0.1 Torr, corresponding fluorescence waveforms are shown in Fig. 5 (a) and (b). Due to the low pressure, the fluorescence intensity is weaker and noiser compared to the 10 Torr case. Through the same fitting procedure, the time constant is obtained as $1/(A+Q)$= 29 ns. Now the decay rates (= $A+Q$ = $A+kN$) has been obtained under different pressures, 10 torr and 0.1 torr, and A and k can be estimated as A = 3.4×10^{7} 1/s and k = 1.3×10^{-16} m^3/s.

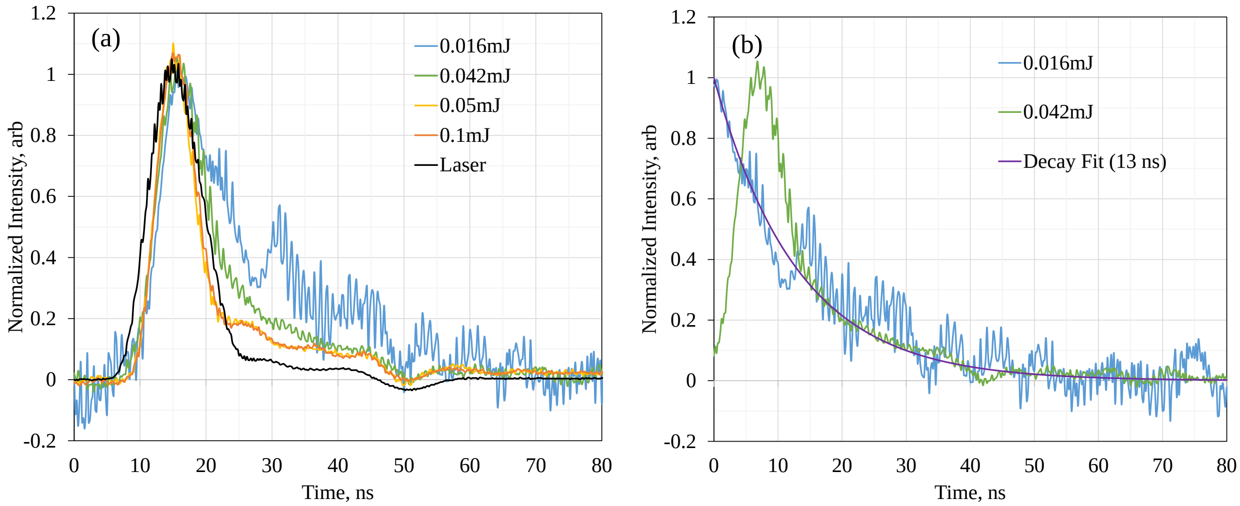

Figure 4. Fluorescence waveforms with 249 nm excitation and 10 Torr pressure. (a) All waveforms with laser pulse. (b) Exponential decay fitting.

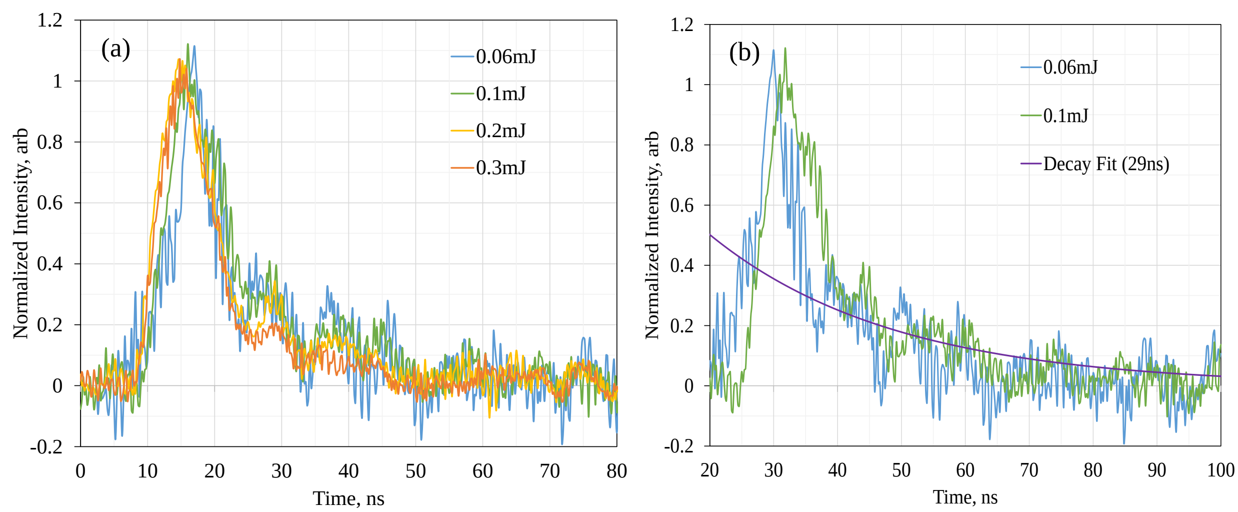

Figure 5. Fluorescence waveforms with 249 nm excitation and 0.1 Torr pressure. (a) All waveforms with laser pulse. (b) Exponential decay fitting.

In the case of weak excitation, because the fluorescence characteristics follows Eq. (7), the fluorescence ratio with the same laser intensity and different pressure can be obtained from A and k using following expression.

$$\frac{S_{F1}}{S_{F2}} = \frac{\dfrac{N_1 I^2}{kN_1 + A}}{\dfrac{N_2 I^2}{kN_2 + A}} = \frac{N_1}{N_2}\frac{kN_2 + A}{kN_1 + A} \qquad (9)$$

where the subscripts 1 and 2 indicate values under 10 Torr and 0.1 Torr, respectively. S_{F1}/S_{F2} = 45 is obtained as a result.

Figure 6 shows the fluorescence response plotted against laser intensity on a logarithmic scale. Here the fluorescence signal is taken to be the time integral of the fluorescence waveform shown in previous figures. The standard error of the fluorescence signal is given in the graph, however, they are not significant – less than 1 % in almost all cases and about 10 % even at minimum laser energy. The power meter used in the experiment is meant for high-powers, thus, the horizontal error is dominant at low power region. The weak excitation characteristic is observed with approximately less than 0.1 mJ laser power. In the weak excitation region, the fluorescence signal should be proportional to the square of laser energy following Eq. (7), and S_{F1}/S_{F2} should be 45 as obtained from Eq. (9). A line is described in Fig. 6 to agree with these two conditions and corresponds to the experimental data. As for high power region, 0.1 mJ to 10 mJ, the fluorescence signal still increases with the laser power, that is, saturation is not achieved because spontaneous emission and nonradiative transition take place at same rate (intermediate situation) or only a part of the observation region may achieve saturation due to the non-uniform spatial laser energy distribution.

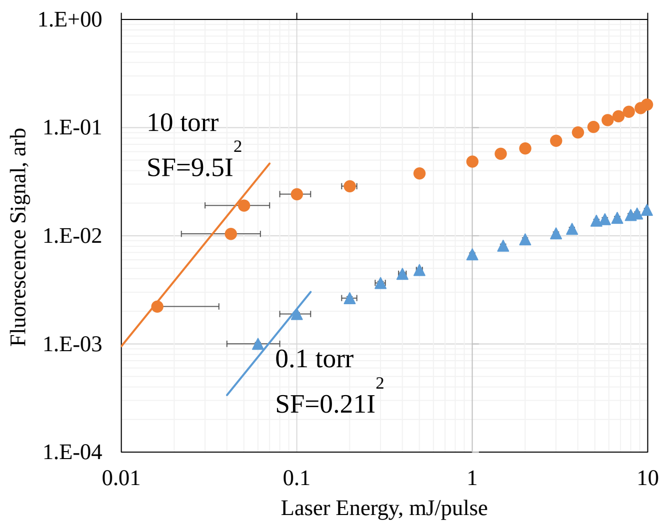

Figure 6. Fluorescence response with 249 nm excitation.

B. 252 nm Laser Excitation

The fluorescence waveforms with 252 nm pumping are shown in Figs. 7 and 8 in the same manner as the case with 249 nm laser wavelength. As a whole, stronger fluorescence intensity is obtained than that with the 249 nm laser, thus, the noise seems to be smaller. The decay time constants are estimated as 12 ns and 25 ns under 10 torr and 0.1 torr, respectively. Consequently, $A = 4.0\times10^{7}$ 1/s and $k = 1.3\times10^{-16}$ m^3/s are obtained.

Figure 9 shows the fluorescence response against laser intensity. $S_{F1}/S_{F2} = 48$ is obtained from Eq. (9), and a line is shown based on this in Fig. 9 which agrees with the experimental data similar to the 249 nm laser case. In contrast to the 249 nm laser wavelength, the saturation condition is obtained at 0.1 Torr with the 252 nm laser.

Table 2 gives *A* and *k* obtained in the present experiments compared with the literature. They show almost the same values which indicates reliability of the experiment.

Table 2. A and k obtained in experiment compared with literatures

Excited state		1/*A*, ns	*k*, 10^{-17} m3/s
6p $[1/2]_0$ (249 nm)	Exp	29±6	13±3
	Ref 12	28	6.0
6p $[3/2]_2$ (252 nm)	Exp	25±5	13±3
	Ref 13	35	11
	Ref 14	30	8.7

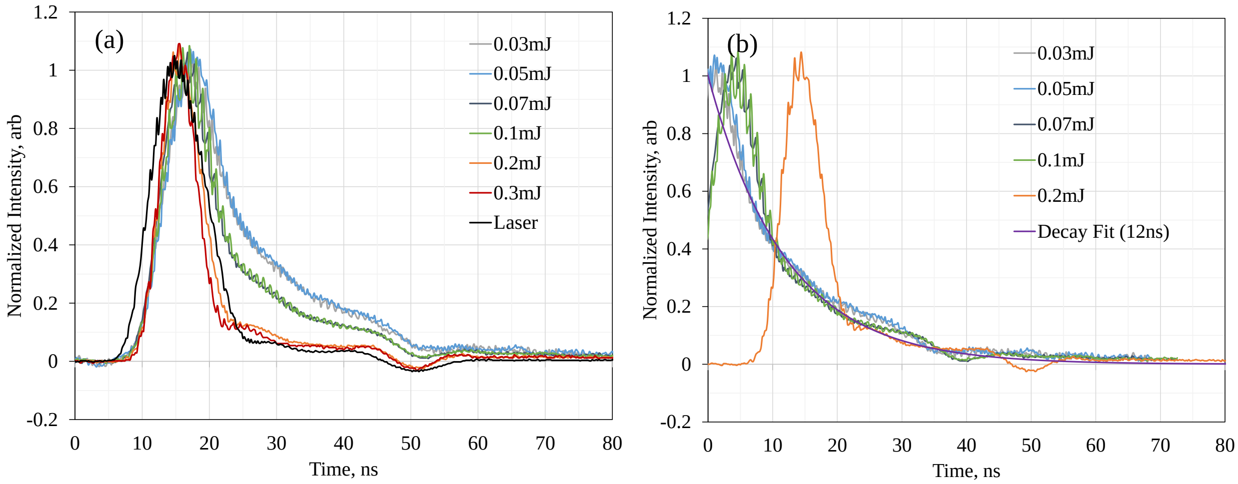

Figure 7. Fluorescence waveforms with 252 nm excitation and 10 Torr pressure. (a) All waveforms with laser pulse. (b) Exponential decay fitting.

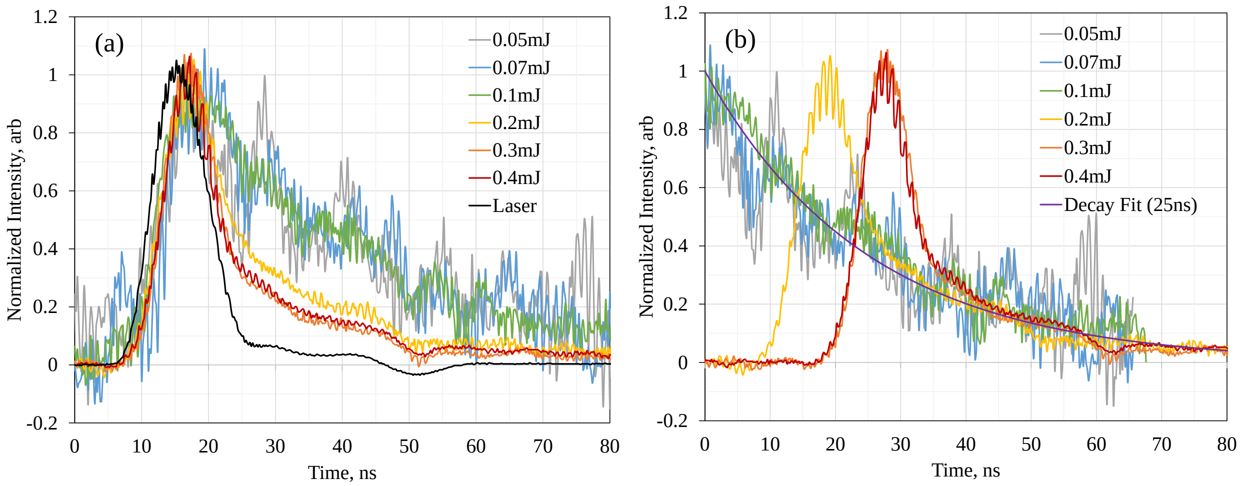

Figure 8. Fluorescence waveforms with 252 nm excitation and 0.1 Torr pressure. (a) All waveforms with laser pulse. (b) Exponential decay fitting.

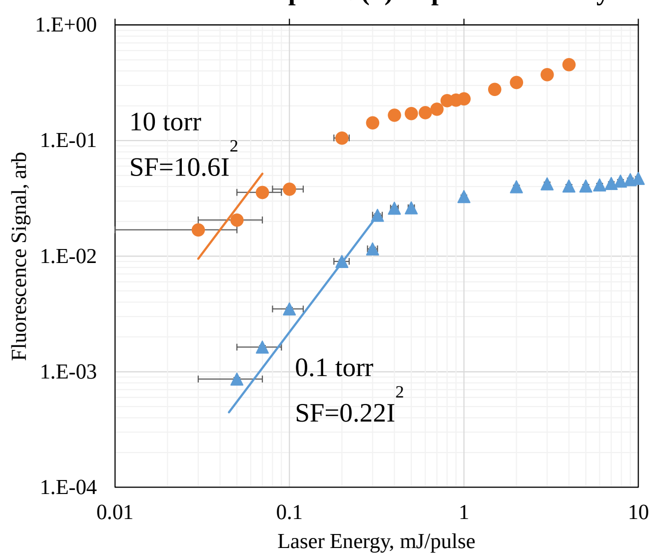

Figure 9. Fluorescence response with 252 nm excitation.

V. Investigation of Application to Hall Thrusters

Application of TALIF to measure neutral xenon density around ion engines and hall thrusters has been investigated in the literature[6-8]. TALIF has already been applied to a hall thruster[5] and that has provided useful information. However, the measurement was conducted within the plume region with the observation that the fluorescence was saturated. To extend the application of TALIF to investigation of ion generation, observation inside the discharge channel, etc., it is necessary to obtain the TALIF characteristics over a suitable range of pressures, that is, approximately 0.1 to 10^{-5} Torr. An optimization of incident laser energy is necessary for each experimental condition, therefore, applying TALIF for neutral xenon density measurement in and around hall thrusters will be discussed for both the weak-excitation and saturation regimes based on the present experimental results with 252 nm laser excitation. Density measurements using the intermediate situation would be difficult because of the complex fluorescence response.

A. Saturation Fluorescence

As shown in Fig. 9, the saturation condition has been achieved around 10 mJ laser energy in the case of 0.1 Torr, and the fluorescence signal is about 0.05. On the other hand, as shown in Figs. 6 and 9, the fluorescence signals still increase with the laser energy even with 10 mJ in other conditions, that means the saturation condition have been never achieved. Under saturation conditions, the pressure ratio should correspond to fluorescence signal ratio in theory seen in Eq. (8), but in fact, no such trend is observed in the experimental result. Thus, achieving true saturation would suggest large and high cost laser systems because of the strong laser energy requirements.

The target pressure range for Hall thrusters would be 0.1 to 10^{-5} Torr and $A \gg Q = kN$ in this condition. Hence, $(B_{02} + B_{20})I^2 \gg Q + A \approx A$ should be satisfied to achieve saturation so that required laser energy would be constant in the pressure range and it would be around 10 mJ as seen in the experiment. The expected fluorescence signal at the lowest pressure, 10^{-5} Torr, would be 5×10^{-6} because the fluorescence signal is proportional to the number density. Fluorescence signal of 5×10^{-4} can be detected by means of the photo detector in the current setup, however, photo multiplier tube (PMT) is necessary to detect 5×10^{-6}. By using PMT, fluorescence can be detected even with the low pressure conditions, but it requires higher cost and plasma and stray emissions must be blocked or filtered because of PMT's high sensitivity.

There would be several ways to calibrate the fluorescence signal versus neutral xenon density. In Ref. 4, the xenon gas was injected from the thruster without discharge, then TALIF observations and pressure measurements with an ionization gauge were conducted around the thruster and compared. In addition to this, the measured density distribution was integrated along the cross-section of the channel, and compared against the xenon mass flowrate assuming a thermal velocity distribution.

B. Weak Excitation Fluorescence

In the weak-excitation regime, high sensitivity fluorescence detection would be required as the fluorescence signal decreases by about one order of magnitude compared to the saturation regime, but correspondingly, one or two orders less laser energy can be applied, that is, even 1 mJ or 0.1 mJ laser energy would be applicable. That is a great advantage of the weak excitation because the large scale and low cost laser system to achieve the saturation would not be necessary. Besides, for observation of high pressure region like 0.1 Torr, the photo detector can be used, that means, smaller scale optical setup could be built. As for low pressure region, PMT would be still necessary and achievement of the saturation would be inevitable in some cases depending on the accuracy of fluorescence detection system.

To obtain xenon number density with the weak excitation, A and k should be estimated because the fluorescence signal follows Eq. (7). In general, k depends on temperature, or proportional to the thermal velocity, however, in the target pressure range $A \gg Q = kN$ is achieved. Thus, Eq. (7) becomes

$$S_F = V\frac{\Omega}{4\pi}A_{21}N\frac{B_{02}I^2}{A} \qquad (10)$$

S_F is simply proportional to NI^2. That means the calibration is possible with fluorescence observation under known pressure in the same way as the saturation condition. Necessity of estimating k may seem a disadvantage for weak excitation, but regarding ion engines and Hall thrusters, the requirement may not be considered for the time being as stated earlier.

Temperature dependence of two-photon absorption cross section due to Doppler broadening is discussed in Ref. 7, the result shows there would be 62 % difference for neutral xenon density measurements between 293 K and 6000 K. In Ref. 15, translational temperature of oxygen atom has been measured using Doppler broadening of the TALIF spectrum. This temperature measurement would be applicable to xenon as well.

To achieve high accuracy, plasma emission from the thruster should be considered. Investigation of detected emission difference between with and without incident laser, S/N ratio of fluorescence and plasma emission, etc., would be needed to select appropriate laser and observation wavelengths. The accuracy of the number density depends on the effect of plasma emission, detection sensitivity and way of calibration. They should be carefully taken into account for electric propulsion applications.

VI. Conclusion

TALIF characteristics were obtained with 249 and 252 nm laser excitation at xenon pressures of 0.1 and 10 Torr. A and k were estimated from the time constants of fluorescence decay in the experiment, and the results are in good agreement with the literature. The fluorescence signal was measured against a wide range of laser energies, and the fluorescence response, characteristics of the weak-excitation, intermediate and saturation regimes, were successfully obtained. In consistent with theory, the weak-excitation regime yields the most accurate predictions of A and k.

Application of TALIF to ground tests of Hall thrusters has been investigated based on these experimental results. It is easier to detect the fluorescence signal under saturation regime, but high power and high cost laser would be required to fully saturate the signal. In fact, the saturation condition has not been attained even with 10 mJ/pulse in the experiment in some cases. The weak excitation may require a PMT in order to detect the fluorescence signal, but has an advantage that low power lasers are applicable. In terms of observation inside discharge channels, where higher xenon density is achieved than that in the plume region, photo detectors used in the experiment could be used, that means the measurement would be realizable with a small scale setup. In general, the weak excitation has a disadvantage that estimation of the quenching rate constant k is required. However, for the current operation range of electric propulsion, the estimation is not necessary. To achieve high accuracy, consideration of effect of the background emission, optimization of laser and observation wavelengths, temperature correction and robust calibration methods are necessary.

References

[1] Tsukizaki, R., Koizumi, H., Nishiyama, K. and Kuninaka, H., “Measurement of Axial Neutral Density Profiles in a Microwave Discharge Ion Thruster by Laser Absorption Spectroscopy with Optical Fiber Probes,” Review of Scientific Instruments 82, 123103, 2011.

[2] Yamamoto, Y., Tsukizaki, R., Yamagiwa, Y., Kanda, T., Nishiyama, K. and Kuninaka, K., “Ion Velocity Measurement with Laser Induced Fluorescence in Microwave Discharge Ion Engine Plume,” ISAS/JAXA Space Transportation Symposium, STEP-2016-067, 2017. In Japanese.

[3] Chng, T. L., and Miles, R. B., “A Comparison of Radar REMPI and Laser Induced Fluorescence for Concentration Measurements,” AIAA paper 2016-1700, 2016.

[4] Crofton, M. W., Hsu Schouten, A. G., Young, J. A., Beiting, E. J., Diamante, K. D., Corey and Delgado, J. J., “Neutral Xenon Density in the SPT-140 Near-Field Plume,” IEPC paper 2013-399, 2013.

[5] Mazouffre, S., Kulaev, V. and Luna, J., “Ion Diagnostics of a Discharge in Crossed Electric and Magnetic Fields for Electric Propulsion", IOP Plasma Source Sci. Technol. 18, 034022, 2009.

[6] Eichhorn, C., Winter, M., Auweter-Kurtz, M., and Lohle, S., “Multi-Photon Spectroscopy on Xenon for Application Ion Thruster Plasma Parameter Investigations: Experiment and Theory,” IEPC paper 2007-169, 2007.

[7] Semenova, M., Auweter-Kurtz, M., and Winter, M., “Development of Laser-spectroscopic Techniques on Xenon for RIT-Ion Thruster Plume Investigations,” AIAA paper 2004-3962, 2004.

[8] Crofton, M. W., “Measurement of Neutral Xenon Density Profile in an Ion Thruster Plume,” AIAA paper 96-2290.

[9] Chng, T. L., and Miles, R. B., “Understanding the Impact of Buffer Gases on the Radar REMPI Diagnostic,” AIAA paper 2015-2803, 2015.

[10] Kröll, S., amd Bischel, W. K., “Two-photon Absorption and Photoionization Cross-section Measurements in the $5p^5 6p$ Configuration of Xenon,” Physical Review A, Vol. 41, No. 3, 1990.

[11] Bednar, N. J., “Development of a Spatially Resolved Optical Technique to Measure Temperature using Two-Photon Absorption of Xenon,” MSc. Thesis, University of Wisconsin-Madison, 2005.

[12] Alford, W. J., “State-to-state rate constants for quenching of xenon 6p levels by rare gases,” J. Chem. Phys., 96 (6), 15 March 1992.

[13] Alford, W. J., “Quenching of $6p[3/2]_1$ and $6p[5/2]_2$ Levels of Atomic Xenon by Rare Gases,” IEEE Journal of Quantum Electronics, 26(9), 1633-1638.

[14] Gessel, A. F. H., Grootel, S. C., and Bruggeman, P. J., “Atomic oxygen TALIF measurements in an atmospheric-pressure microwave plasma jet with in situ xenon calibration,” Plasma Sources Sci. Technol. 22 (2013) 055010.

[15] Takayanagi, T., Kato, S., Mizuno, M., Fujii, K., Fujita, K., Matsui, M. and Yamagiwa, Y., “ Flow Temperature Measurement of Arc Wind Tunnel with Laser Induced Fluorescence,” ISAS/JAXA Space Flight Dynamics Symposium, 2013. In Japanese.